Annual Review of Physical Chemistry

In Situ Measurement of Evolving Excited-State Dynamics During Deposition and Processing of Organic Films by Single-Shot Transient Absorption

Zachary S. Walbrun[1] and Cathy Y. Wong[1,2]

[1]Department of Chemistry and Biochemistry, University of Oregon, Eugene, Oregon, USA

[2]Oregon Center for Optical, Molecular, and Quantum Science, and Material Science Institute, University of Oregon, Eugene, Oregon, USA; email: cwong3@uoregon.edu

Annu. Rev. Phys. Chem. 2023. 74:267–86

First published as a Review in Advance on February 28, 2023

The *Annual Review of Physical Chemistry* is online at physchem.annualreviews.org

https://doi.org/10.1146/annurev-physchem-102722-041313

Keywords

transient absorption, in situ spectroscopy, instrument design, organic thin film, molecular aggregation, thermal annealing

Abstract

A significant advantage of organic semiconductors over many of their inorganic counterparts is solution processability. However, solution processing commonly yields heterogeneous films with properties that are highly sensitive to the conditions and parameters of casting and processing. Measuring the key properties of these materials in situ, during film production, can provide new insight into the mechanism of these processing steps and how they lead to the emergence of the final organic film properties. The excited-state dynamics is often of import in photovoltaic, electronic, and light-emitting devices. This review focuses on single-shot transient absorption, which measures a transient spectrum in a single shot, enabling the rapid measurement of unstable chemical systems such as organic films during their casting and processing. We review the principles of instrument design and provide examples of the utility of this spectroscopy for measuring organic films during their production.

1. INTRODUCTION

TA: transient absorption

SSTA: single-shot transient absorption

OPV: organic photovoltaics

OLED: organic light-emitting diode

PL: photoluminescence

Transient absorption (TA) is a time-resolved spectroscopy that can provide insight into the electronic structure and exciton dynamics of chemical systems. This review focuses on an implementation of TA called single-shot transient absorption (SSTA) that permits rapid and accurate measurement of exciton dynamics during the formation and processing of organic films. After briefly motivating the study of organic semiconductors and describing the impact of film deposition on the resulting film photophysics, we review SSTA instrumentation and illustrate the insights that can be gleaned by applying this spectroscopy during organic film formation and processing.

Organic semiconducting materials show great promise for organic photovoltaic (OPV) and organic light-emitting diode (OLED) applications owing to their solution processability, compatibility with flexible substrates, and chemical tunability (1–6). Organic semiconductors are excitonic materials owing to their relatively low dielectric constants, with electron–hole binding energies in the hundreds of millielectronvolts. Excitons are photogenerated in OPV materials, and the constituent electrons and holes must overcome their binding energy to become charge separated before they can migrate to electrodes. This is typically accomplished with a combination of organic materials, one an electron donor and the other an electron acceptor, so that excitons encountering an interface between these two materials may split to form a charge transfer state. This physical separation can lower the binding energy and promote further separation of charges. Conversely, charges are injected into an OLED device, and electrons and holes must migrate, meet, and recombine to emit a photon (7). Thus, many molecules in OLED devices are designed to promote photoluminescence (PL) by tuning spin-orbit coupling, the relative energies of singlet and triplet states, and the transition rates between them (8, 9).

Both OPVs and OLEDs are reaching commercial viability. The efficiency of OPVs has historically lagged behind other types of photovoltaics, with a slow rate of efficiency improvement (10) despite significant research efforts. However, the development of nonfullerene electron acceptors over the past decade is driving a rejuvenation of interest. The first single-junction OPV using a nonfullerene acceptor to exceed the champion efficiency of a fullerene-based device was at 13.1% in 2017 (11), and efficiencies have climbed rapidly since then, with an efficiency of 19.2% reported in 2022 (12). Meanwhile, OLEDs are already found in televisions and cell phones, leveraging their energy efficiency, brightness, and large field of view. They are also thinner and lighter than traditional LEDs and can be deposited onto flexible plastic substrates, which may enable their usage in wearable electronics and health care devices such as biosensors and phototherapeutics (13–15).

Solution processability is one of the primary potential benefits of organic semiconductors. Some of the many methods that can be used to deposit solutions of organic semiconductors (16) are shown in **Figure 1**. Dropcasting and spincoating are commonly used in academic research laboratories to produce small-area films. Dropcasting involves casting a solution on a substrate and allowing the solvent to evaporate, oftentimes resulting in a coffee-ring effect (17) and nonuniform films. Spincoating, in which solution is deposited onto a spinning substrate and excess solution is flung away to leave a thin film, results in more uniform films (16, 18), but a significant amount of solution is wasted. Printing processes using a brush, spray nozzle, blade, or slot-die are amenable to roll-to-roll production methods that can rapidly yield large-area films (3, 19, 20). Manufacturing these films on a large scale could increase manufacturing speed, decrease cost, and require less energy compared with the methods used to produce all-inorganic devices (21).

While solution processing can be faster, cheaper, and less energy intensive, the result is also more heterogeneous. Different intermolecular orientations and film morphologies can become kinetically trapped, depending on deposition method and subsequent film processing. For example, a spincoated film is typically in its final form within a few seconds, whereas a dropcasted film may require minutes to hours to completely dry, depending on the solvent boiling point.

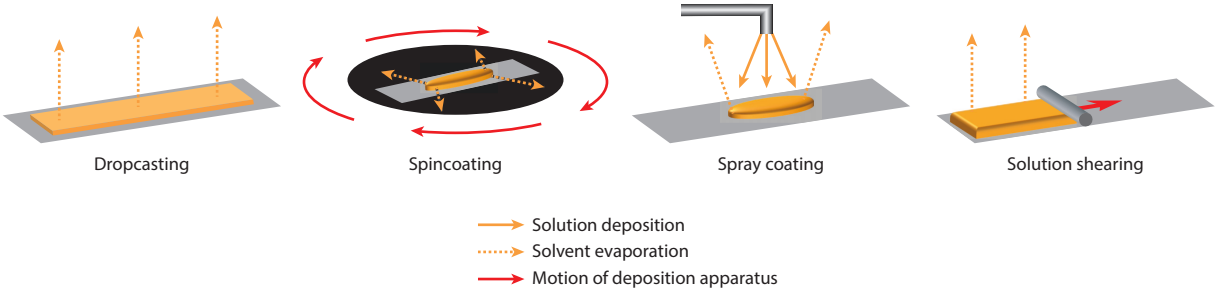

Figure 1

Film deposition techniques. Solid orange arrows and dashed orange arrows represent solution deposition and solvent evaporation, respectively, and red arrows show motion of deposition apparatus.

When solvent leaves the film rapidly, the remaining organic molecules can adopt kinetically trapped packing structures, resulting in fewer ordered aggregates (22, 23). Variations in molecular arrangement and the resulting distribution of electronic coupling between organic molecules can dramatically affect the wave functions and energies of the electronic states, as well as the transition rates between them. This can result in exciton or carrier traps and other local geometries that affect dynamics, exciton migration, and charge transport. Postdeposition processing techniques such as thermal or solvent annealing can modify photophysics by increasing the number of ordered aggregates (24–27). In a film with multiple components, such as the electron donor and acceptor in an OPV, deposition and postprocessing can also affect the structure and extent of the interface between the two systems. Changes to this interface can affect exciton diffusion, charge transfer, and charge separation (26, 28, 29). Understanding how the electronic structure and excited-state dynamics evolve during film deposition and processing may aid in the design of scalable manufacturing methods to yield optimal behavior. The remainder of this review focuses on SSTA, an implementation of TA that can enable measurements of excited-state dynamics during organic film formation and processing.

2. TRANSIENT ABSORPTION AND SINGLE-SHOT TRANSIENT ABSORPTION

2.1. Transient Absorption

TA is a time-resolved pump-probe spectroscopy that can measure the transition rates between stationary states in a sample. Many different implementations of TA are possible, but the critical components of a TA instrument are shown in **Figure 2*a***. A pulsed laser is used to excite the sample and probe the absorption of the excited sample. The time resolution of the instrument is optimized by compressing the laser pulses with a prism compressor, grating compressor, or chirped mirrors. The output from the laser is typically split with a beam splitter, with one of the resulting beams serving as the pump and the other as the probe. The pump pulse energy must be sufficient to excite a small population of excitons in the sample, with typically <1% of the absorbers excited within the measured sample volume (30). A parametric amplifier can tune the wavelength of the pump pulses to be resonant with the sample to generate a population of excited species. The probe pulse typically has a broadband spectrum generated by focusing into some solid, transparent medium (vide infra), but it can also have a narrower band for so-called one-color measurements. This probe pulse interacts with the sample at some time after the pump generates excited species. The time delay between the pump pulse and the probe pulse is often

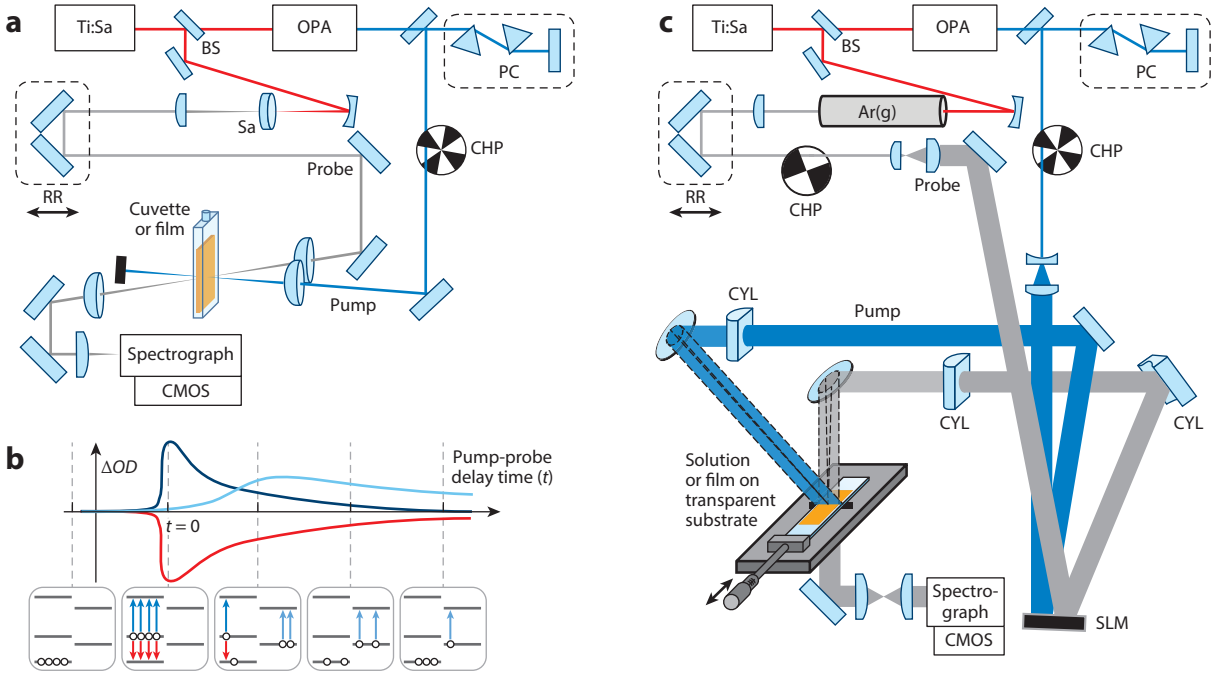

Figure 2

(*a*) Typical TA apparatus. (*b*) Differential optical density can comprise SE (*red lines*), ESA by various excited species (*dark* and *light blue lines*), and GSB (not shown). (*c*) SSTA apparatus. Either lenses or curved mirrors can be used in these instruments, with reflective focusing optics improving attainable time resolution. Panel *c* adapted with permission from Reference 40; copyright 2020 Optical Society of America. Abbreviations: Ar(g), pressurized argon gas cell; BS, beam splitter; CHP, optical chopper; CMOS, complementary metal oxide semiconductor; CYL, cylindrical lens; ESA, excited-state absorption; GSB, ground-state bleach; OPA, optical parametric amplifier; PC, prism compressor; RR, retroreflector; SE, stimulated emission; SLM, spatial light modulator; SSTA, single-shot transient absorption; TA, transient absorption; Ti:Sa, titanium:sapphire laser.

controlled with a retroreflector on a high-precision motorized translation stage. The pump pulse toggles between being blocked and being let through to the sample by way of an optical chopper. Both the pump pulse and the probe pulse are focused to a spot on the sample, and the transmitted probe is sent to a spectrograph, which typically consists of a dispersive grating and a detector array. TA signal is the change in transmission (ΔT) owing to illumination by the pump pulse. This can then be converted to differential optical density: $\Delta OD = -\log(\Delta T/T + 1)$.

Ground-state bleach, stimulated emission, and excited-state absorption comprise the resulting signal, which can provide information on the excited-state dynamics of a sample (**Figure 2*b***). TA measurements can elucidate the growth and decay of populations of nonemissive excited states after photoexcitation, which steady-state spectroscopy cannot provide (31–39). The limitation of traditional TA is that measurements at each pump-probe time delay occur in series, typically by translating the retroreflector between each measurement. As a result, many minutes to a few hours of measurement are typically required to achieve a reasonable signal-to-noise ratio (SNR). This limits traditional TA to the study of systems that are stable for the duration of that measurement.

SNR: signal-to-noise ratio

2.2. Strategies for Single-Shot Transient Absorption

SSTA addresses the limitations of traditional TA instruments by simultaneously measuring signal at a range of pump-probe time delays. The two primary strategies for spatial encoding are depicted

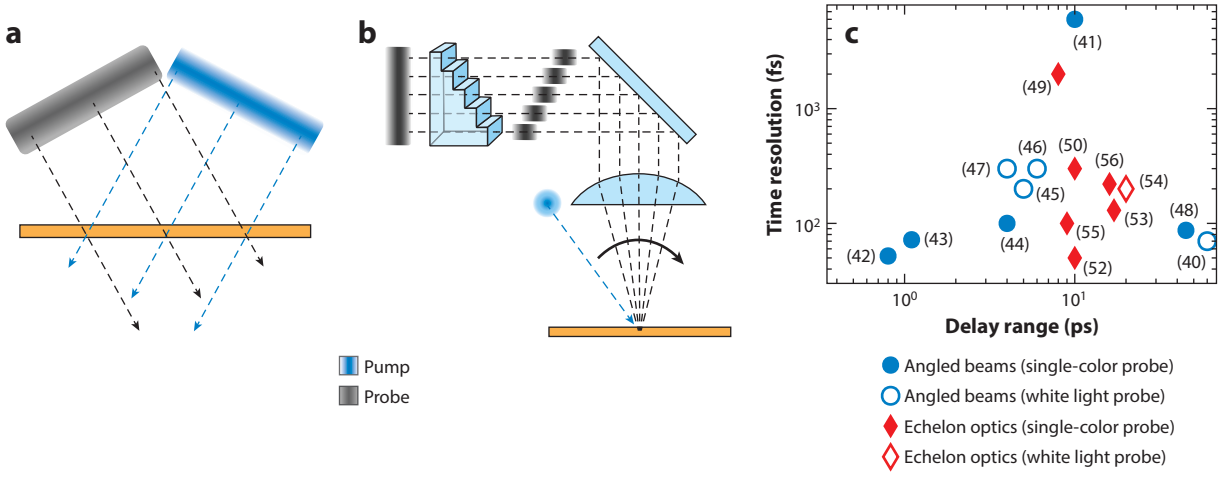

Figure 3

Angled beams (*a*) or echelon optics (*b*) can be used to spatially encode the time delay between the pump (*blue*) and the probe (*gray*), with dashed lines showing the beam propagation direction. (*c*) Time delay and time resolution reported for instruments utilizing angled beams (*blue circles*) and echelon optics (*red diamonds*). Unfilled and filled shapes represent instruments that use a white light probe and a single-color probe, respectively. Corresponding references are shown in parentheses. Figure adapted with permission from Reference 57; copyright 2021 Elsevier B.V.

in **Figure 3**. Angled beams can spatially encode the time delay at the sample position (40–48), or transmissive or reflective echelons can encode the time delay at the back focal plane of the lens prior to the sample (49–56). The time delay between the pump and the probe must vary as a function of location in the sample plane (**Figure 3*a***) or the back focal plane (**Figure 3*b***), and the probe beam at that plane must be imaged onto an array detector after it has passed through the sample. When spatial encoding occurs at the back focal plane, the pump and probe pulses can then be focused to a spot at the sample plane, as is typical for a traditional TA measurement. When spatial encoding occurs at the sample plane, the measured area must be larger, which enables higher pulse energies to be used and can improve the SNR, but it requires a relatively spatially homogeneous sample. **Figure 3*c*** shows the time delay range and time resolution of broadband and one-color SSTA instruments reported in the literature using these strategies.

3. INSTRUMENTATION FOR SINGLE-SHOT TRANSIENT ABSORPTION

The fundamental elements of an SSTA instrument (**Figure 2*c***) are similar to those of a traditional TA instrument (**Figure 2*a***), with a few notable differences. Here, we focus on spatially encoding the pump-probe time delay at the sample plane, similar to **Figure 3*a***, but some of the issues discussed below also apply to spatial encoding in the back focal plane.

3.1. Controlling Time Delay Range and Resolution

The range of the pump-probe time delay is $t_{\text{range}} = d\ sin\theta/c$, where d is the length of the line of overlap between the pump and the probe at the sample position, θ is the angle between the pump and the probe wave fronts, and c is the speed of light (**Figure 4*a***). Longer lines of overlap on the sample enable greater pump-probe time delay ranges (**Figure 4*c***), but the desire to measure a longer line of sample must be tempered with the increased pulse energy, optic size, and sample size

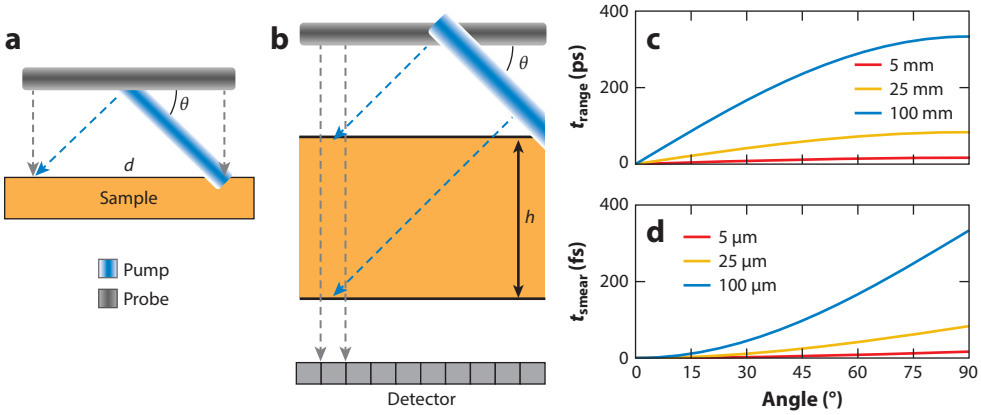

Figure 4

(*a*) Schematic illustrating parameters that determine time delay. (*b*) Pump-probe time delay is different at the top and bottom of a column of sample that is measured with a single detector pixel, resulting in loss of time resolution. (*c*) Time range for three different overlap line lengths at the sample and (*d*) time smear for three different film thicknesses as a function of angle between the pump pulse and the probe pulse.

needed. Although the angle between the beams can be increased to elongate the pump-probe time delay range, this increase can also reduce the time resolution, particularly when measuring thick samples (**Figure 4*d***). The column of sample traversed by a particular region of the probe beam will have been excited by different regions of the pump beam (**Figure 4*b***). This effectively smears the pump-probe time delay within the thickness of the sample. The extent of this smearing is $t_{smear} = h(1 - cos\theta)/c$, where h is the sample thickness. Note that this is a simplified expression that does not account for the refractive index of the sample (57). If t_{smear} is less than the duration of the pump pulse itself, the sample thickness and angle will not have much impact on the time resolution. The angle can thus be chosen with the sample thickness, pulse duration, and anticipated dynamics in mind to optimize the time delay range and resolution. For example, as typical time constants are in the tens to hundreds of picoseconds for exciton diffusion, and as fast as 100 fs for charge separation (58), t_{smear} should be <100 fs if these processes are of interest. **Figure 4*d*** illustrates that a 100-μm film will not limit the time resolution of an instrument if $\theta < 45°$. Films with $h < 25$ μm will not have a significant impact on the time resolution for any θ. For measurements during film deposition, the thickness of the layer of deposited solution, which is significantly thicker than the resulting film, may affect the time resolution.

The resulting spatially encoded pump-probe time delay range is imaged onto an array detector. If a broadband probe is used, the light will be dispersed by a spectrograph prior to arrival at the detector. Thus, each two-dimensional image contains a transient spectrum, and the time delay and wavelength reported by each pixel are determined by a calibration procedure reported elsewhere (40).

3.2. Pulse Energy

Measuring a line of sample in an SSTA instrument requires more pulse energy than that required for the equivalent measurement of a spot in a typical TA instrument. Ideally, the pump should excite an organic film to near the upper limit of its linear regime, such that the SNR can be optimal while avoiding exciton–exciton interactions. The energy density required for this can vary widely for different organic systems, from <10 to >400 μJ/cm^2 (59–63). Even at the high end of this range, a pump pulse need be only 0.3 μJ for a 300-μm spot, typical for a traditional TA

instrument. However, if the pump is spread over a line 20 mm × 300 μm for angled-beam SSTA, the required pulse energy becomes 25 μJ. Some higher-repetition-rate femtosecond-laser systems may not be able to deliver the required pulse energy after accounting for the conversion efficiency of an optical parametric amplifier and energy losses at the optics that interact with the pump.

The need for increased pulse energies also applies to the probe. A pulsed white light continuum for broadband TA measurements is typically generated by focusing the fundamental of a femtosecond laser into a crystal of sapphire or calcium fluoride (64). The conversion efficiency of the incident pulse at its original wavelength to the broadband pulse is typically quite low, for example, only ~2% in sapphire (57). Despite this low efficiency, sapphire can produce sufficient broadband pulse energies for TA measurements of small sample spots. In any spatially encoded SSTA measurement the probe pulse must be imaged onto multiple pixels, with each pixel encoding some particular pump-probe delay time. Thus, more probe photons are necessary to achieve a similar SNR. The simplest way to increase the energy of the broadband pulse for a spatially encoded SSTA measurement is to increase the pulse energy input into the sapphire. However, when the laser-induced damage threshold of the material is exceeded, the intense electric field of femtosecond-laser pulses can induce avalanche ionization in solid media, which irreversibly damages the material. Although sapphire has a relatively high damage threshold (5–10 J/cm^2 using 100-fs pulses) (65), it cannot generate adequate broadband pulse energy for measurements using a spatially encoded time delay without damage.

Damage can be avoided and adequate broadband probe energies can be achieved with nonsolid media for continuum generation. High pulse energies have been reported when generation occurs in liquid jets (66–68) and in gas cells (69). Although the conversion efficiency may be significantly lower than in solid media, their resistance to avalanche ionization enables the use of intense input pulses that more than compensate for the lower conversion inefficiency. Continuum generation in an argon gas cell is an example of this. Continuum generation occurs over a short distance at the center of a >1-m-long cell, with long focal lengths into and out of the cell preventing damage to the input and output cell windows. Factors such as focal length, the diameter of an iris before the cell, pulse duration, gas pressure, and gas identity affect conversion efficiency and spectral stability for a gas cell (57, 70). Although the efficiency of a gas cell may be well under 1%, this is offset by the increased input energy, yielding an output energy that is sufficient for SSTA measurements.

3.3. Beam Flattening

Use of a spatially encoded pump-probe time delay for accurate TA measurements requires that both the pump and the probe have a relatively flat spatial profile at the plane where spatial encoding occurs, either the sample plane or the back focal plane. If a Gaussian spatial profile is used, a larger population of excited species will be photogenerated for pump-probe time delays encoded by the middle of a focal line or the middle of the back focal plane. This could result in different dynamics owing to interactions between these excited species (e.g., exciton–exciton annihilation), which would make the spatially encoded measurement inaccurate. Those same areas would then be measured with larger probe intensity, yielding a greater SNR, whereas the edges of the spatially encoded region would be measured with weaker probe intensity and have a lower SNR. This is the primary reason why many of the SSTA instruments shown in **Figure 3*c*** have such short pump-probe time delay ranges: In these instruments, only the central, relatively flat portion of a Gaussian beam profile is utilized for the spatially encoded time delay. The time delay range can be expanded by flattening the spatial profile of the pump and probe pulses so that the pulse energy is equally distributed over the measured line of sample.

If the input beam is close to Gaussian, commercially available aspherical lenses can shape the beam to a top-hat spatial profile, which can be used in the back focal plane of an imaging system,

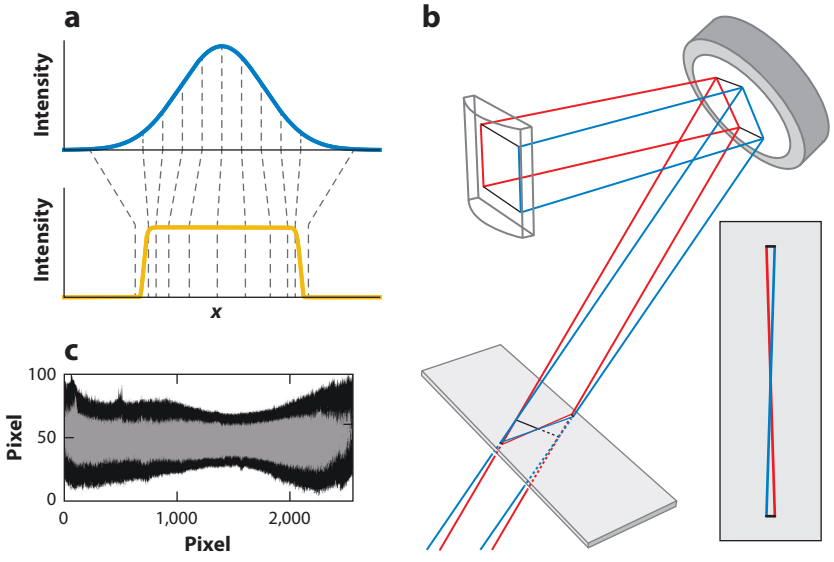

Figure 5

(*a*) Intensity of a Gaussian spatial beam profile can be redistributed into a top-hat spatial profile with an SLM. Panel *a* adapted with permission from Reference 48; copyright 2018 Optical Society of America. (*b*) Pump beam focused to the sample plane with a cylindrical lens. Inset shows a top-down view of the bowtie shape at the sample plane. Panel *b* adapted with permission from Reference 40; copyright 2020 Optical Society of America. (*c*) Pump beam imaged with fluorescent sample showing initial bowtie shape (*black*) and after imparting variable focal length (*gray*). Abbreviation: SLM, spatial light modulator.

or the beam can be further focused to a flat line with a cylindrical optic. If the initial beam profile is not adequately Gaussian, the output from this optical system may not be adequately flat. In this case, geometric beam shaping can be performed on both the pump pulse and the probe pulse with a phase-only spatial light modulator (SLM). Variable phase is imparted to light that interacts with each pixel of the SLM, which can cause the SLM to act similarly to a lens or prism, adjusting the convergence and translation of parts of the beam (**Figure 5*a***). Although the phase map needed to shape an imperfect Gaussian profile to a top hat is not analytically known, numerical methods can be applied to get close to an even spatial profile (48). Calibration and normalization can account for any small remaining variations in the spatial profile of either the pump or the probe, so long as the measured sample is excited in the linear regime (40). However, postprocessing of the data cannot change the SNR measured at different locations. When a pump beam with a nonuniform spatial profile is used, the areas with lower incident energy density will have a lower density of excited species and thus a reduced SNR. Similarly, the regions measured with lower probe energy will also suffer from a lower SNR. Thus, measurements will have a better SNR when a closer-to-perfect top-hat spatial profile and incident power close to the upper limit of the linear excitation regime are used.

If the pump is focused to a line to spatially encode the time delay, one subtle consideration is that the pump pulse energy should ideally be uniform over both the length and the width of the line projected by the pump onto the sample. If the pump pulse is not incident normal to the sample, the focal line produced by a cylindrical lens will also be angled relative to the sample. Thus, even if the pump is focused to a perfectly evenly illuminated line, its projection onto the sample plane will appear to be shaped like a bowtie, with more energy density at the center than at the

SLM: spatial light modulator

edges (**Figure 5*b***). The overall pulse energy would have to be lowered to avoid exciton–exciton interactions at the center, lowering the measured SNR at the edges. This is an argument for using an SLM rather than a simple aspheric lens to shape the beam, as its phase map can be modified to provide variable focal length lensing to avoid the bowtie shape at the sample plane (57). The pump beam is difficult to image directly, but a fluorescent sample can be used to determine the intensity profile of the beam before and after implementing variable focal length with an SLM (**Figure 5*c***).

4. CONSIDERATIONS DURING MEASUREMENT OF DYNAMIC, ORGANIC SYSTEMS

Interrogation of evolving organic systems using SSTA presents a few unique challenges when compared with traditional TA. In this section, we discuss the need for dynamic background correction, the need for spatial heterogeneity, the need to adapt deposition and processing techniques for in situ measurement, and the utility of multimodal measurements.

4.1. Dynamic Background Correction

Traditional TA measurements utilize a single optical chopper in the pump beamline so that the transmission of the probe pulse with (T_1) and without (T_0) pump photoexcitation of the sample can be measured and compared to yield the differential transmission ($\Delta T = T_1 - T_0$). Any light that is incident on the detector but is not altered by the presence of the pump (e.g., ambient light) will not be included in ΔT. The pump itself, however, can cause additional detected light that is unrelated to the differential transmission. In particular, the pump can cause sample PL and scatter, and if any of this light is incident on the detector, it will contribute to the apparent ΔT because it is also modulated by the presence or absence of the pump. As the pump-induced PL and scatter do not change as a function of pump-probe delay time, the contribution of this light to ΔT is not typically a significant issue: The constant baseline in the measured transients can be simply subtracted during data processing. These contributions are more problematic if they vary as a function of the pump-probe delay, as may be the case for a spatially encoded time delay, and if these contributions change as a function of real time, as is likely for an evolving sample. An additional optical chopper placed in the probe beamline can allow these background contributions to be subtracted for each measured transient. If the frequency of the chopper in the pump beam is double or half that of the chopper frequency in the probe beam, all four possible combinations of the pump and probe pulses can be detected: T_{11}, T_{10}, T_{01}, and T_{00}, where $T_{\text{pump probe}}$ is the transmission, 0 represents a blocked pulse, and 1 is a pulse incident on the sample. T_{10} accounts for the pump-induced scatter and PL, and T_{00} is signal present when neither pump nor probe is incident on the sample, including dark current and ambient light (71). The differential transmission can be calculated as

$$\frac{\Delta T}{T} = \frac{(T_{11} - T_{10}) - (T_{01} - T_{00})}{(T_{01} - T_{00})} \qquad 1.$$

and then converted to ΔOD.

This correction technique is critical when measuring evolving organic films, as the PL and scatter are likely to undergo significant changes, as demonstrated in **Figure 6**. The PL detected from a sulforhodamine solution varies spatially, resulting in a varying contribution to the ΔT signal as a function of a spatially encoded time delay as opposed to appearing as a constant baseline. Thus, its contribution must be measured separately and subtracted. The PL decreases significantly when the molecules aggregate to form a thin film, thus requiring its contribution to be continually measured during any change from solution to film. Additionally, the film may have small structural features that cause pump scatter, and these contributions must also be subtracted. Films are more

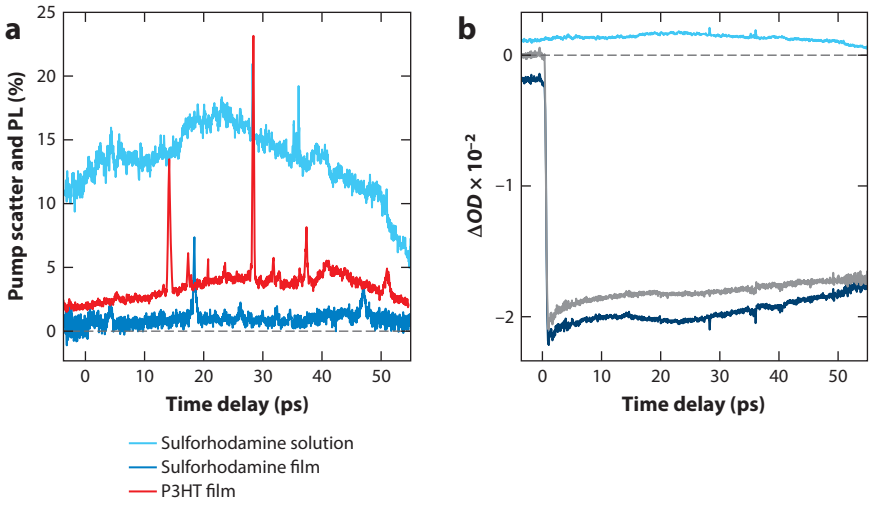

Figure 6

(*a*) Contribution of pump scatter and PL to the detected ΔT for a sulforhodamine solution (*light blue trace*), sulforhodamine film (*blue trace*), and P3HT film (*red trace*). (*b*) Transients before (*dark blue trace*) and after (*gray trace*) correction are shown for sulforhodamine solution with the pump scatter and PL overlaid (*light blue trace*). Figure adapted from Reference 71; copyright 2019 Elsevier B.V. Abbreviations: OD, optical density; P3HT, poly(3-hexylthiophene-2,5-diyl); PL, photoluminescence.

likely to cause pump scatter, as shown for a film of poly(3-hexylthiophene-2,5-diyl) (P3HT). Note that scatter subtraction does not entirely eliminate the impact of scatter. As TA is the measure of a very small signal (ΔT) on top of a large transmission signal, a large dynamic range is needed. Scatter consumes some of that dynamic range, leaving less for the signal from transmission and the small fraction that comprises the differential transmission (71).

The incorporation of dual choppers to measure these background contributions also increases the time needed to perform each measurement and thus the time needed to attain an adequate SNR. However, each individual corrected transient still only requires a few milliseconds, and the measurement will be accurate as long as the sample does not significantly change during those few milliseconds. Averaging multiple spectra will still accurately report the dynamics during that averaged time period.

4.2. Spatial Heterogeneity

The spikes in the scatter contributions in **Figure 6*a*** illustrate the spatial heterogeneity that is possible in organic films. This does not pose a problem for SSTA measurements if the pump-probe time delay is spatially encoded at the back focal plane, as the same sample volume will be measured for each time delay. Heterogeneity can, however, pose a problem if the time delay is encoded at the sample plane. In this type of SSTA measurement, each pixel of the detector corresponds to a particular region of the sample, and that pixel reports the ensemble TA measurement for some particular pump-probe time delay. Thus, heterogeneity within each small sample volume is averaged in that ensemble measurement and does not present a problem. On the other hand, heterogeneity between the small sample volumes does present a significant problem, as the dynamics within each small volume may be different and thus the transient built from a series of these small volumes would not be accurate. A motorized actuator can be used to translate the sample during a measurement to effectively increase the size of the ensemble being measured by

P3HT: poly(3-hexylthiophene-2,5-diyl)

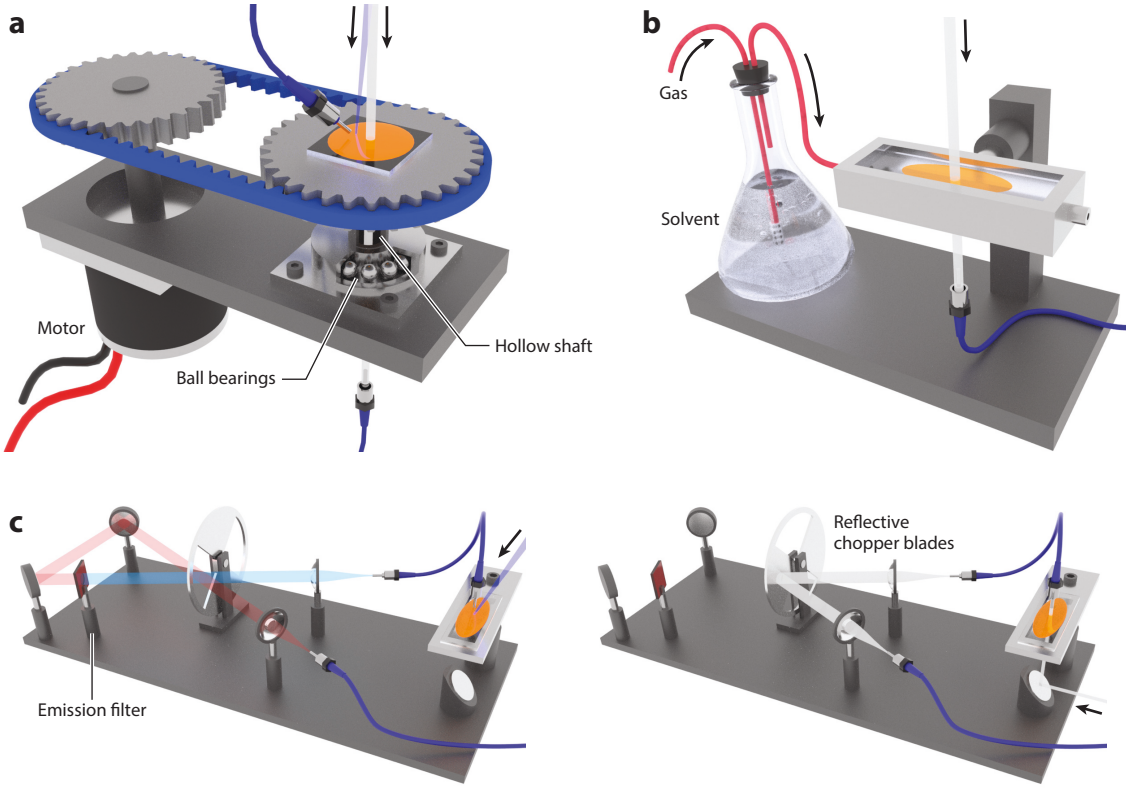

Figure 7

Illustrations of in situ optical spectroscopies. (*a*) Concurrent absorbance and PL measurements on two locations of a sample during spincoating. Substrate spins on a hollow shaft, through which optical measurements can occur. Rotation is actuated by a motor connected by a timing belt. (*b*) Absorbance measurement during solvent vapor annealing. Carrier gas is bubbled through solvent and passes through a sample cell with two transparent faces. (*c*) Method for in situ measurement of absorbance and PL on a single spot on a sample by synchronizing the alternating light sources with a reflective chopper blade so that the two measurements do not interfere with each other and both are detected by the same spectrometer. Panel *c* adapted with permission from Reference 74; copyright 2018 American Chemical Society. Abbreviation: PL, photoluminescence.

each pixel (71, 72). The rate and distance needed for sample translation depend on the size of the spatial features in the sample and the number of pixels onto which the probe is imaged.

4.3. Adapting Deposition and Processing to Perform In Situ Measurements

Performing in situ optical measurements during film formation or processing requires that light be incident on the film and on a detector. Some methods of film casting and processing can be difficult to adapt to transmissive measurement. For example, light cannot be transmitted through the metal chuck of a typical spincoater, which holds the substrate and is driven by a motor. Homebuilt spincoaters (**Figure 7*a***) can be creatively designed to circumvent this problem with the use of the motor to drive a pulley, which actuates and spins a second pulley with a hollow center (73, 74). Processing methodologies such as annealing can also be adapted to optical measurements (24). For example, as shown in **Figure 7*b***, the solvent can pass through a cell with two opposing transparent faces. If the film is deposited on one internal transparent face, optical measurements can be conducted during solvent annealing (75). Transmissive measurements can also be conducted

during thermal annealing, as discussed in Section 5.2, by constructing an electrical heating stage with a hole in the stage surface to allow optical transmission (76).

4.4. Incorporating Multimodal Measurement

Many types of optical spectroscopy are amenable to in situ measurement during the formation and processing of organic films. In situ linear absorbance, reflectance, PL, optical ellipsometry, Raman, and IR spectroscopic measurements have all been reported (24, 73–75, 77–84) during some change in an organic film sample. Additionally, in situ X-ray scattering measurements can provide incredible structural insights into film formation (85–88). Utilizing multiple modalities of in situ measurement yields a more complete picture of both the evolving structure and the photophysics of organic systems. However, the process of film formation and the morphology of the resulting films are often different from one film to the next. Thus, the multiple modalities should optimally measure the same film deposition. Otherwise, the different measurements could be reporting on quite different film formation processes, and their results should not be correlated. Creative instrument design strategies can enable multimodal measurements during film formation (79, 81). For example, **Figure 7*a*** illustrates the concurrent measurement of absorption and PL. Note that the two measurements in this example occur at slightly different locations on the film to prevent scatter from the white light source from contaminating the PL measurement. However, as discussed above, organic films are also commonly spatially heterogeneous. The precise morphology of the film on two measured spots may not be the same. Multiple optical measurements can occur on the same spot on the sample when strategies such as that shown in **Figure 7*c*** are used (74). The white light source and excitation laser for absorbance and PL measurements can be alternately switched on, and transmission of the white light and sample emission after photoexcitation are collected by the same fiber and collimated with a lens. A controller synchronizes these light sources with the phase of an optical chopper with reflective blades, transmitting the PL and reflecting the white light. The transmitted PL can then pass through an emission filter before passing through the optical chopper again. Both the white light and the PL are focused and collected by the same fiber after the optical chopper and measured with the same spectrometer. This enables rapid, alternating measurements of the same spot on the sample while also ensuring that the white light used for the absorbance measurement does not contaminate the PL measurement.

5. IN SITU TRANSIENT ABSORPTION RESULTS

In situ measurements such as those described in Section 4.4 can yield insight into the evolving structure and the absorptive and emissive electronic states of the molecules in the film during deposition. But when the excited-state dynamics is of critical importance, for example, in materials used for photovoltaic or light-emitting devices, time-resolved measurements are key. The purpose of performing measurements in situ is to develop a deeper understanding of what is actually happening during these film formation processes and how that affects the excited-state dynamics of the eventual film. This can also enable the use of dynamic deposition and processing conditions to target particular film characteristics. In this section we provide two examples that demonstrate the utility of in situ measurement of organic films during deposition and processing.

5.1. TA During Organic Film Formation

One of the primary potential benefits of using organic molecules for semiconducting devices is their ability to be deposited to form thin films from solution. Performing measurements during film deposition can give us some unique insights into the process of film formation. Our laboratory reported on PL and TA during the dropcasting of an organic cyanine dye, pseudoisocyanine

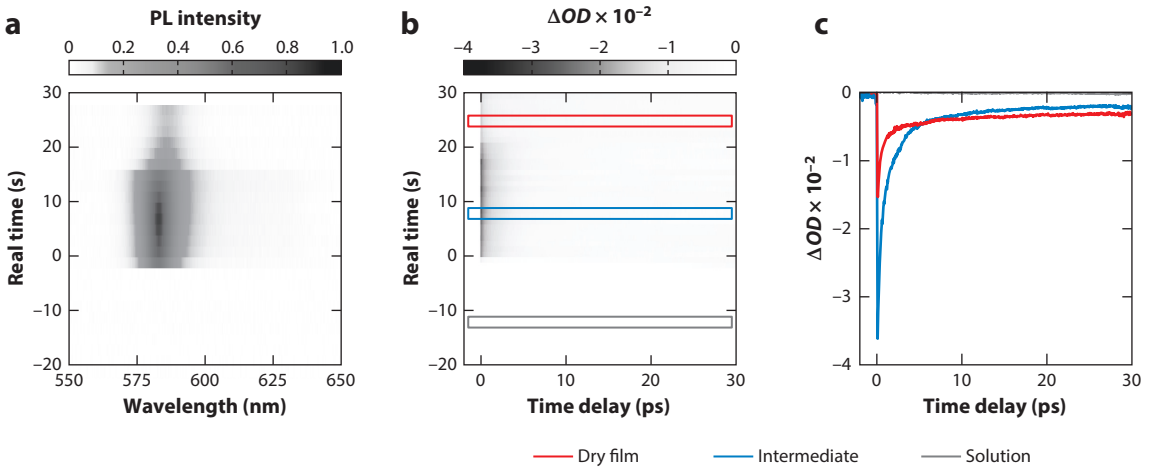

Figure 8

(*a*) PL and (*b*,*c*) SSTA measurements during film formation of PIC. Color of transients in panel *c* correspond to time windows highlighted in panel *b*. Figure adapted with permission from Reference 72; copyright 2018 American Chemical Society. Abbreviations: OD, optical density; PIC, pseudoisocyanine; PL, photoluminescence; SSTA, single-shot transient absorption.

(PIC) (72). We observed that although a solution of PIC in acetone did not exhibit significant PL and the eventual dry thin film was only weakly luminescent, the samples were highly emissive for a short period of time during the process of film formation (**Figure 8*a***). When the solutions were deposited at 13°C, this intermediate stage of the film formation process persisted for only ~20 s. It is difficult, if not impossible, to measure the excited-state dynamics of the molecules during this intermediate stage with a traditional TA instrument that performs measurements at different pump-probe time delays sequentially. The excited-state dynamics could be measured with excellent SNR in 1 s with the use of tilted pulses to spatially encode the time delay into a line at the sample position and with a single-color probe. This enabled TA measurements during the short-lived intermediate stage of film formation (**Figure 8*b*,*c***), revealing unique dynamics during this stage. The transient measured during each 1-s time interval could be fit to triexponentials, revealing dynamics that are fairly constant during each stage of film formation but that change dramatically between stages. The appearance of a new ~100-ps decay component in the excited-state dynamics coincident with the quenching of the strong emission suggests the formation of nonemissive trap states or the weakening of the electronic coupling that initially enhanced J-aggregate behavior. Additional measurements of sample mass during film formation show that the aggregates are still solvated during the intermediate stage, suggesting that interaggregate contact and contact with the substrate upon loss of solvation cause the new quenching process observed in the dynamics. The evolving lineshape of the absorbance spectra could be explained only by the formation of a mixture of H- and J-aggregates during film formation, and the electronic coupling between molecules decreased concurrent with the appearance of the new quenching process (89). These results raise the possibility that PIC could be cast into a highly emissive film if the intermediate stage of film formation could be kinetically trapped. These insights into the process of film formation would not be possible without multimodal in situ measurements (72).

PIC: pseudoisocyanine

5.2. TA During Thermal Annealing of Donor-Acceptor Systems

Various processing steps are often utilized to improve the characteristics of organic thin films after casting. Thermal annealing is a common treatment that can allow organic molecules and polymers

to form larger, more well-ordered crystalline domains, which often results in greater carrier mobility. In situ measurements during thermal annealing can aid in our fundamental understanding of this process and its impact on the photophysics and structure of thin films. We measured the evolving excited-state dynamics during thermal annealing of a prototypical semiconducting polymer, P3HT, for which in situ TA measurements have yet to be reported. We utilized an electric heating stage with a slit at its center to allow for transmissive optical measurements. We ramped the temperature from 30°C to 140°C in steps of 10°C every 5 min. The heating stage was then turned off and further TA measurements were conducted as the sample cooled back to 30°C.

The transient spectra measured during heating and cooling were each globally fit to a biexponential function. The amplitude associated with the shorter time constant from the global fit is plotted as a function of temperature in **Figure 9*c***. The transient spectra during thermal annealing are quite different from the spectrum either before or after annealing. This is further emphasized in the spectral slices of **Figure 9*d***; the spectral features of the transient spectrum at 140°C are not part of a simple progression between the features of the pre- and postannealing spectra. The excited-state dynamics during thermal annealing is also not simply an intermediate between the dynamics measured pre- and postannealing. The shorter time constant (τ_1) became shorter during heating but then partially recovered as the sample cooled (**Figure 9*e***). Other features

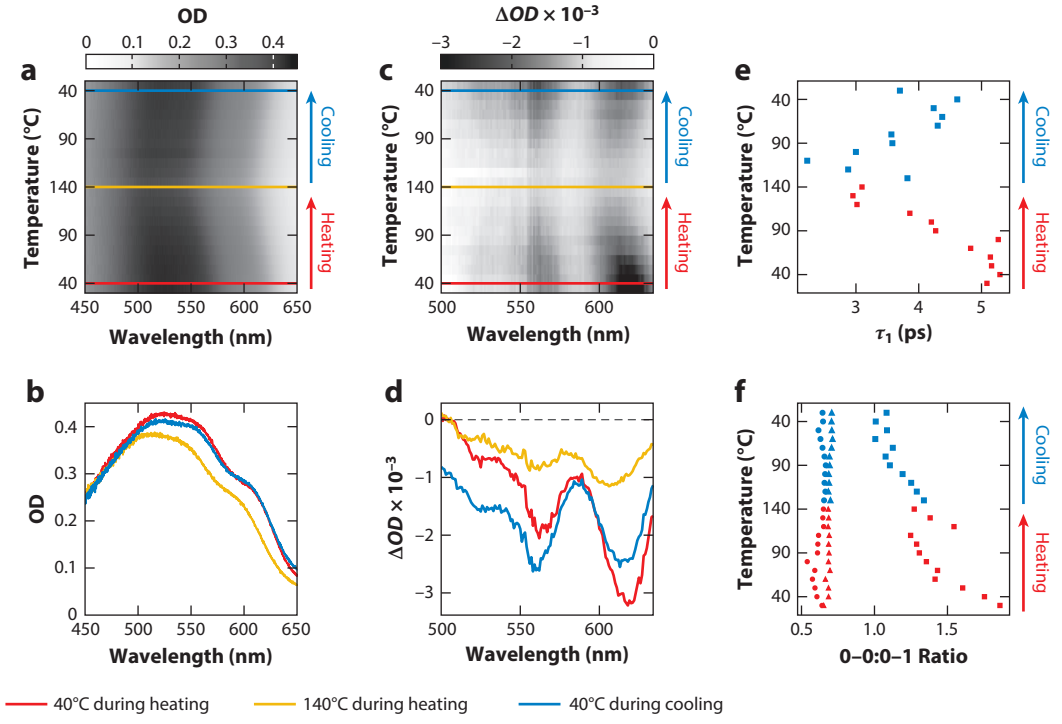

Figure 9

Linear absorbance and SSTA measurements during heating and cooling of a P3HT film. Linear absorbance (*a*) and slices at time points during annealing (*b*), indicated with colored lines in panel *a*. (*c*) Amplitude A_1 associated with the short time constant τ_1 from global fitting as a function of annealing and cooling temperature. (*d*) Spectral slices at time points during thermal annealing as indicated by colored lines in panel *c*. (*e*) Time constant τ_1 of the fastest exponential component in global fits to the transients. (*f*) Intensity ratio of the 0–0 peak to the 0–1 peak in amplitudes A_1 and A_2, associated with the shorter (*squares*) and longer (*circles*) time constants and linear absorbance (*triangles*), as a function of annealing progress. Abbreviations: OD, optical density; P3HT, poly(3-hexylthiophene-2,5-diyl); SSTA, single-shot transient absorption.

followed one trend throughout the heating and cooling process, for example, the intensity ratio of the 0–0 peak to the 0–1 peak in the amplitude spectrum associated with τ_1 (**Figure 9*c***) decreases steadily, as shown in **Figure 9*f***, indicating increased H-aggregate behavior in the species that produces the τ_1 decay during both heating and cooling. However, the same trend in the 0–0:0–1 ratio is not observed in the amplitude associated with the longer time constant nor in the linear absorbance (**Figure 9*f***). The species that exhibits increased H-aggregation during annealing is revealed only through SSTA. Emergence of unique dynamics and transient spectra during the annealing process indicates that some phenomena other than the steady formation of H-aggregates must be occurring. Further multimodal in situ measurements and analysis of these data may shine a new light on how processing techniques such as thermal and solvent annealing proceed and how these techniques might be modified to target particular excited-state dynamics.

6. SUMMARY AND OUTLOOK

The photophysics of organic thin films is of great consequence to their potential application in semiconducting devices and is dramatically influenced by the method and details of their deposition and subsequent processing. Developing a deeper understanding of how these formation and processing steps affect the electronic structure and excited-state dynamics of organic systems can provide inspiration for modified deposition and processing techniques to target desired photophysics. SSTA can be used to reveal how the excited-state dynamics of organic films emerges during their formation and processing. In reviewing the technical underpinnings of SSTA instruments, we highlighted some of the concerns most relevant to the measurement of organic films. We also provide some examples of in situ measurements that reveal unique excited-state dynamics during film formation and processing that is not merely a weighted sum of the dynamics measured before and after these fabrication processes. SSTA could also be used to study other dynamic processes in organic materials, for example, during photodamage, self-healing, or photochemical reactions. In particular, SSTA can measure the dynamics of molecules prior to photochemistry that would otherwise be caused by many minutes of traditional TA measurement.

Improving some of the limitations of SSTA will broaden the applicability of this technique, the questions it can answer, and the likelihood of more widespread adoption. Methods using customized optics to expand the pump-probe time delay range that can be acquired in a single shot will expand the excited-state dynamics that can be probed. Creative encoding of the time delay away from the sample plane would alleviate the need for sample homogeneity and could even enable diffraction-limited spatial resolution, which would dramatically increase the questions that SSTA could address. Improved algorithms for flattening the pump profile and new methods for directly imaging that profile would enable easier calibration and make SSTA more user-friendly. As demonstrated in this review, SSTA has joined the suite of in situ measurements that can provide new insight into how excited-state dynamics emerges during chemical and structural changes in organic films. The scientific questions that can be addressed by SSTA will continue to grow as further innovations enhance the technique.

SUMMARY POINTS

1. Single-shot transient absorption can measure excited-state dynamics in a few milliseconds, with a good signal-to-noise ratio in organic films achievable in a few seconds.
2. Tilted pulses or echelon optics can spatially encode a pump-probe time delay.

3. Flattening of spatial profile and pulse energies is a primary concern when using angled beams.
4. Dynamic background correction, averaging over heterogeneity, and adaptation of film fabrication techniques for optical measurements are primary concerns when measuring organic thin films.
5. Excited-state dynamics that emerges during fabrication but does not persist in final organic films can provide insight into the mechanism of fabrication process.

DISCLOSURE STATEMENT

The authors are not aware of any affiliations, memberships, funding, or financial holdings that might be perceived as affecting the objectivity of this review.

ACKNOWLEDGMENTS

This material is based on work supported by the National Science Foundation under grant 1752129.

LITERATURE CITED

1. Mainville M, Leclerc M. 2020. Recent progress on indoor organic photovoltaics: from molecular design to production scale. *ACS Energy Lett.* 5(4):1186–97
2. Ng LWT, Lee SW, Chang DW, Hodgkiss JM, Vak D. 2022. Organic photovoltaics' new renaissance: advances toward roll-to-roll manufacturing of non-fullerene acceptor organic photovoltaics. *Adv. Mater. Technol.* 7(10):2101556
3. Sampaio PGV, González MOA, de Oliveira Ferreira P, da Cunha Jácome Vidal P, Pereira JPP, et al. 2020. Overview of printing and coating techniques in the production of organic photovoltaic cells. *Int. J. Energy Res.* 44(13):9912–31
4. Salehi A, Fu X, Shin D, So F. 2019. Recent advances in OLED optical design. *Adv. Funct. Mater.* 29(15):1808803
5. Wadsworth A, Moser M, Marks A, Little MS, Gasparini N, et al. 2019. Critical review of the molecular design progress in non-fullerene electron acceptors towards commercially viable organic solar cells. *Chem. Soc. Rev.* 48(6):1596–625
6. Wadsworth A, Hamid Z, Kosco J, Gasparini N, McCulloch I. 2020. The bulk heterojunction in organic photovoltaic, photodetector, and photocatalytic applications. *Adv. Mater.* 32(38):2001763
7. Luscombe CK, Maitra U, Walter M, Wiedmer SK. 2021. Theoretical background on semiconducting polymers and their applications to OSCs and OLEDs. *Chem. Teach. Int.* 3(2):169–83
8. Chen D, Li W, Gan L, Wang Z, Li M, Su S-J. 2020. Non-noble-metal-based organic emitters for OLED applications. *Mater. Sci. Eng. R Rep.* 142:100581
9. Mahoro GU, Fernandez-Cestau J, Renaud J, Coto PB, Costa RD, Gaillard S. 2020. Recent advances in solid-state lighting devices using transition metal complexes exhibiting thermally activated delayed fluorescent emission mechanism. *Adv. Opt. Mater.* 8(16):2000260
10. Meredith P, Li W, Armin A. 2020. Nonfullerene acceptors: a renaissance in organic photovoltaics? *Adv. Energy Mater.* 10(33):2001788
11. Zhao W, Li S, Yao H, Zhang S, Zhang Y, et al. 2017. Molecular optimization enables over 13% efficiency in organic solar cells. *J. Am. Chem. Soc.* 139(21):7148–51
12. Zhu L, Zhang M, Xu J, Li C, Yan J, et al. 2022. Single-junction organic solar cells with over 19% efficiency enabled by a refined double-fibril network morphology. *Nat. Mater.* 21(6):656–63
13. Hong G, Gan X, Leonhardt C, Zhang Z, Seibert J, et al. 2021. A brief history of OLEDs—emitter development and industry milestones. *Adv. Mater.* 33(9):2005630

14. Song J, Lee H, Jeong EG, Choi KC, Yoo S. 2020. Organic light-emitting diodes: pushing toward the limits and beyond. *Adv. Mater.* 32(35):1907539
15. Huang Y, Hsiang E-L, Deng M-Y, Wu S-T. 2020. Mini-LED, Micro-LED and OLED displays: present status and future perspectives. *Light Sci. Appl.* 9(1):105
16. Diao Y, Shaw L, Bao Z, Mannsfeld SCB. 2014. Morphology control strategies for solution-processed organic semiconductor thin films. *Energy Environ. Sci.* 7(7):2145–59
17. Larson RG. 2017. Twenty years of drying droplets. *Nature* 550(7677):466–67
18. Hall DB, Underhill P, Torkelson JM. 1998. Spin coating of thin and ultrathin polymer films. *Polym. Eng. Sci.* 38(12):2039–45
19. Yang F, Huang Y, Li Y, Li Y. 2021. Large-area flexible organic solar cells. *NPJ Flex Electron.* 5(1):30
20. Wang G, Adil MA, Zhang J, Wei Z. 2019. Large-area organic solar cells: material requirements, modular designs, and printing methods. *Adv. Mater.* 31(45):1805089
21. Carlé JE, Helgesen M, Hagemann O, Hösel M, Heckler IM, et al. 2017. Overcoming the scaling lag for polymer solar cells. *Joule* 1(2):274–89
22. Seifrid MT, Oosterhout SD, Toney MF, Bazan GC. 2018. Kinetic versus thermodynamic orientational preferences for a series of isomorphic molecular semiconductors. *ACS Omega* 3(8):10198–204
23. Rivnay J, Steyrleuthner R, Jimison LH, Casadei A, Chen Z, et al. 2011. Drastic control of texture in a high performance n-type polymeric semiconductor and implications for charge transport. *Macromolecules* 44(13):5246–55
24. Miller S, Fanchini G, Lin Y-Y, Li C, Chen C-W, et al. 2008. Investigation of nanoscale morphological changes in organic photovoltaics during solvent vapor annealing. *J. Mater. Chem.* 18(3):306–12
25. Marsh RA, Hodgkiss JM, Albert-Seifried S, Friend RH. 2010. Effect of annealing on P3HT:PCBM charge transfer and nanoscale morphology probed by ultrafast spectroscopy. *Nano Lett.* 10(3):923–30
26. Zhang Y, Sajjad MT, Blaszczyk O, Parnell AJ, Ruseckas A, et al. 2019. Large crystalline domains and an enhanced exciton diffusion length enable efficient organic solar cells. *Chem. Mater.* 31(17):6548–57
27. Cui C, Li Y. 2021. Morphology optimization of photoactive layers in organic solar cells. *Aggregate* 2:e31
28. Serbenta A, Kozlov OV, Portale G, van Loosdrecht PHM, Pshenichnikov MS. 2016. Bulk heterojunction morphology of polymer:fullerene blends revealed by ultrafast spectroscopy. *Sci. Rep.* 6(1):36236
29. Markov DE, Amsterdam E, Blom PWM, Sieval AB, Hummelen JC. 2005. Accurate measurement of the exciton diffusion length in a conjugated polymer using a heterostructure with a side-chain cross-linked fullerene layer. *J. Phys. Chem. A* 109(24):5266–74
30. Berera R, van Grondelle R, Kennis JTM. 2009. Ultrafast transient absorption spectroscopy: principles and application to photosynthetic systems. *Photosynth. Res.* 101(2–3):105–18
31. Bakulin AA, Dimitrov SD, Rao A, Chow PCY, Nielsen CB, et al. 2013. Charge-transfer state dynamics following hole and electron transfer in organic photovoltaic devices. *J. Phys. Chem. Lett.* 4(1):209–15
32. Ohkita H, Cook S, Astuti Y, Duffy W, Tierney S, et al. 2008. Charge carrier formation in polythiophene/fullerene blend films studied by transient absorption spectroscopy. *J. Am. Chem. Soc.* 130(10):3030–42
33. Kandada ARS, Grancini G, Petrozza A, Perissinotto S, Fazzi D, et al. 2013. Ultrafast energy transfer in ultrathin organic donor/acceptor blend. *Sci. Rep.* 3(1):2073
34. Hartnett PE, Dyar SM, Margulies EA, Shoer LE, Cook AW, et al. 2015. Long-lived charge carrier generation in ordered films of a covalent perylenediimide-diketopyrrolopyrrole-perylenediimide molecule. *Chem. Sci.* 6(1):402–11
35. Falke SM, Rozzi CA, Brida D, Maiuri M, Amato M, et al. 2014. Coherent ultrafast charge transfer in an organic photovoltaic blend. *Science* 344(6187):1001–5
36. Rana A, Sharma C, Prabhu DD, Kumar M, Karuvath Y, et al. 2018. Revealing charge carrier dynamics in squaraine:[6, 6]-phenyl-C 71-butyric acid methyl ester based organic solar cells. *AIP Adv.* 8(4):045302
37. Hinrichsen TF, Chan CCS, Ma C, Paleček D, Gillett A, et al. 2020. Long-lived and disorder-free charge transfer states enable endothermic charge separation in efficient non-fullerene organic solar cells. *Nat. Commun.* 11(1):5617
38. Dong Y, Cha H, Bristow HL, Lee J, Kumar A, et al. 2021. Correlating charge-transfer state lifetimes with material energetics in polymer:non-fullerene acceptor organic solar cells. *J. Am. Chem. Soc.* 143(20):7599–603

39. Dimitriev OP, Blank DA, Ganser C, Teichert C. 2018. Effect of the polymer chain arrangement on exciton and polaron dynamics in P3HT and P3HT:PCBM films. *J. Phys. Chem. C* 122(30):17096–109
40. Wilson KS, Mapile AN, Wong CY. 2020. Broadband single-shot transient absorption spectroscopy. *Opt. Express* 28(8):11339–55
41. Malley MM, Rentzepis PM. 1969. Picosend molecular relaxation displayed with crossed laser beams. *Chem. Phys. Lett.* 3(7):534–36
42. Salin F, Georges P, Roger G, Brun A. 1987. Single-shot measurement of a 52-fs pulse. *Appl. Opt.* 26(21):4528–31
43. Dhar L, Fourkas JT, Nelson KA. 1994. Pulse-length-limited ultrafast pump-probe spectroscopy in a single laser shot. *Opt. Lett.* 19(9):643–45
44. Fujimoto M, Aoshima S, Tsuchiya Y. 2002. Ultrafast imaging to measure instantaneous intensity distributions of femtosecond optical pulses propagating in a medium. *Meas. Sci. Technol.* 13(11):1698–709
45. Furukawa N, Mair CE, Kleiman VD, Takeda J. 2004. Femtosecond real-time pump-probe imaging spectroscopy. *Appl. Phys. Lett.* 85(20):4645
46. Makishima Y, Furukawa N, Ishida A, Takeda J. 2006. Femtosecond real-time pump-probe imaging spectroscopy implemented on a single shot basis. *Jpn. J. Appl. Phys.* 45(7R):5986
47. Ferrari R, D'Andrea C, Bassi A, Valentini G, Cubeddu R. 2007. Time-gated real-time pump-probe imaging spectroscopy. *Proc. SPIE* 6631
48. Wilson KS, Wong CY. 2018. Single-shot transient absorption spectroscopy with a 45 ps pump-probe time delay range. *Opt. Lett.* 43(3):371–74
49. Topp MR, Rentzepis PM, Jones RP. 1971. Time-resolved absorption spectroscopy in the 10^{-12}-sec range. *J. Appl. Phys.* 42(9):3415–19
50. Wakeham GP, Nelson KA. 2000. Dual-echelon single-shot femtosecond spectroscopy. *Opt. Lett.* 25(7):505–7
51. Wakeham GP, Chung DD, Nelson KA. 2002. Femtosecond time-resolved spectroscopy of energetic materials. *Thermochim. Acta* 384(1):7–21
52. Poulin PR, Nelson KA. 2006. Irreversible organic crystalline chemistry monitored in real time. *Science* 313(5794):1756–60
53. Katayama I, Sakaibara H, Takeda J. 2011. Real-time time-frequency imaging of ultrashort laser pulses using an echelon mirror. *Jpn. J. Appl. Phys.* 50(10R):102701
54. Minami Y, Yamaki H, Katayama I, Takeda J. 2014. Broadband pump-probe imaging spectroscopy applicable to ultrafast single-shot events. *Appl. Phys. Express* 7(2):022402
55. Shin T, Wolfson JW, Teitelbaum SW, Kandyla M, Nelson KA. 2014. Dual echelon femtosecond single-shot spectroscopy. *Rev. Sci. Instrum.* 85(8):083115
56. Yang J, Zhou W, Wang F, Deng K, Yi T, et al. 2020. Single-shot pump-probe technique using mirror array. *Appl. Phys. B* 126(5):98
57. Wilson KS, Walbrun ZS, Wong CY. 2021. Single-shot transient absorption spectroscopy techniques and design principles. *Spectrochim. Acta Part A Mol. Biomol. Spectrosc.* 253:119557
58. Whaley KB, Kocherzhenko AA, Nitzan A. 2014. Coherent and diffusive time scales for exciton dissociation in bulk heterojunction photovoltaic cells. *J. Phys. Chem. C* 118(47):27235–44
59. Piris J, Dykstra TE, Bakulin AA, van Loosdrecht PHM, Knulst W, et al. 2009. Photogeneration and ultrafast dynamics of excitons and charges in P3HT/PCBM blends. *J. Phys. Chem. C* 113(32):14500–6
60. Stevens MA, Silva C, Russell DM, Friend RH. 2001. Exciton dissociation mechanisms in the polymeric semiconductors poly(9,9-dioctylfluorene) and poly(9,9-dioctylfluorene-co-benzothiadiazole). *Phys. Rev. B* 63(16):165213
61. Zarrabi N, Burn PL, Meredith P, Shaw PE. 2016. Acceptor and excitation density dependence of the ultrafast polaron absorption signal in donor-acceptor organic solar cell blends. *J. Phys. Chem. Lett.* 7(14):2640–46
62. Guo J, Ohkita H, Benten H, Ito S. 2009. Near-IR femtosecond transient absorption spectroscopy of ultrafast polaron and triplet exciton formation in polythiophene films with different regioregularities. *J. Am. Chem. Soc.* 131(46):16869–80
63. Kaake LG, Moses D, Heeger AJ. 2013. Coherence and uncertainty in nanostructured organic photovoltaics. *J. Phys. Chem. Lett.* 4(14):2264–68

64. Couairon A, Mysyrowicz A. 2007. Femtosecond filamentation in transparent media. *Phys. Rep.* 441(2):47–189
65. Uteza O, Bussière B, Canova F, Chambaret J-P, Delaporte P, et al. 2007. Laser-induced damage threshold of sapphire in nanosecond, picosecond and femtosecond regimes. *Appl. Surf. Sci.* 254(4):799–803
66. Fork RL, Tomlinson WJ, Shank CV, Hirlimann C, Yen R. 1983. Femtosecond white-light continuum pulses. *Opt. Lett.* 8(1):1–3
67. Tcypkin AN, Putilin SE, Melnik MV, Makarov EA, Bespalov VG, Kozlov SA. 2016. Generation of high-intensity spectral supercontinuum of more than two octaves in a water jet. *Appl. Opt.* 55(29):8390–94
68. Dharmadhikari JA, Steinmeyer G, Gopakumar G, Mathur D, Dharmadhikari AK. 2016. Femtosecond supercontinuum generation in water in the vicinity of absorption bands. *Opt. Lett.* 41(15):3475–78
69. Corkum PB, Rolland C, Srinivasan-Rao T. 1986. Supercontinuum generation in gases. *Phys. Rev. Lett.* 57(18):2268–71
70. Kosma K, Trushin SA, Fuß W, Schmid WE. 2008. Characterization of the supercontinuum radiation generated by self-focusing of few-cycle 800 nm pulses in argon. *J. Mod. Opt.* 55(13):2141–77
71. Wilson KS, Scott MN, Wong CY. 2019. Excited state dynamics of organic semiconductors measured with shot-to-shot correction of scatter and photoluminescence. *Synth. Metals* 250:115–20
72. Wilson KS, Wong CY. 2018. In situ measurement of exciton dynamics during thin-film formation using single-shot transient absorption. *J. Phys. Chem. A* 122(31):6438–44
73. Abdelsamie M, Zhao K, Niazi MR, Chou KW, Amassian A. 2014. In situ UV-visible absorption during spin-coating of organic semiconductors: a new probe for organic electronics and photovoltaics. *J. Mater. Chem. C* 2(17):3373–81
74. Buchhorn M, Wedler S, Panzer F. 2018. Setup to study the in situ evolution of both photoluminescence and absorption during the processing of organic or hybrid semiconductors. *J. Phys. Chem. A* 122(46):9115–22
75. Zomerman D, Kong J, McAfee SM, Welch GC, Kelly TL. 2018. Control and characterization of organic solar cell morphology through variable-pressure solvent vapor annealing. *ACS Appl. Energy Mater.* 1(10):5663–74
76. Walbrun ZS, Leibfried LC, Hoban ÁR, Rasmussen BC, Wiegand TJ, et al. 2022. Effect of thermal annealing on aggregation of a squaraine thin film. *MRS Adv.* 7(12):239–44
77. van Franeker JJ, Turbiez M, Li W, Wienk MM, Janssen RAJ. 2015. A real-time study of the benefits of co-solvents in polymer solar cell processing. *Nat. Commun.* 6(1):6229
78. Shin N, Richter LJ, Herzing AA, Kline RJ, DeLongchamp DM. 2013. Effect of processing additives on the solidification of blade-coated polymer/fullerene blend films via in-situ structure measurements. *Adv. Energy Mater.* 3(7):938–48
79. Güldal NS, Kassar T, Berlinghof M, Ameri T, Osvet A, et al. 2016. Real-time evaluation of thin film drying kinetics using an advanced, multi-probe optical setup. *J. Mater. Chem. C* 4(11):2178–86
80. Sims M, Zheng K, Quiles MC, Xia R, Stavrinou PN, et al. 2005. On the use of optical probes to monitor the thermal transitions in spin-coated poly(9,9-dioctylfluorene) films. *J. Phys. Condens. Matter* 17(41):6307–18
81. Engmann S, Bokel FA, Ro HW, DeLongchamp DM, Richter LJ. 2016. Real-time photoluminescence studies of structure evolution in organic solar cells. *Adv. Energy Mater.* 6(10):1502011
82. Campoy-Quiles M, Alonso MI, Bradley DDC, Richter LJ. 2014. Advanced ellipsometric characterization of conjugated polymer films. *Adv. Funct. Mater.* 24(15):2116–34
83. Ando M, Yoneya M, Kehoe TB, Ishii H, Minakata T, et al. 2019. Disorder and localization dynamics in polymorphs of the molecular semiconductor pentacene probed by *in situ* micro-Raman spectroscopy and molecular dynamics simulations. *Phys. Rev. Mater.* 3(2):025601
84. Schönherr H, Frank CW. 2003. Ultrathin films of poly(ethylene oxides) on oxidized silicon. 1. Spectroscopic characterization of film structure and crystallization kinetics. *Macromolecules* 36(4):1188–98
85. Kim Y-J, Lee S, Niazi MR, Hwang K, Tang M-C, et al. 2020. Systematic study on the morphological development of blade-coated conjugated polymer thin films via in situ measurements. *ACS Appl. Mater. Interfaces* 12(32):36417–27

86. Baran D, Ashraf RS, Hanifi DA, Abdelsamie M, Gasparini N, et al. 2017. Reducing the efficiency-stability-cost gap of organic photovoltaics with highly efficient and stable small molecule acceptor ternary solar cells. *Nat. Mater.* 16(3):363–69
87. Jiang X, Chotard P, Luo K, Eckmann F, Tu S, et al. 2022. Revealing donor-acceptor interaction on the printed active layer morphology and the formation kinetics for nonfullerene organic solar cells at ambient conditions. *Adv. Energy Mater.* 12:2103977
88. Posselt D, Zhang J, Smilgies D-M, Berezkin AV, Potemkin II, Papadakis CM. 2017. Restructuring in block copolymer thin films: in situ GISAXS investigations during solvent vapor annealing. *Prog. Polym. Sci.* 66:80–115
89. Sosa ML, Wong CY. 2020. Revealing the evolving mixture of molecular aggregates during organic film formation using simulations of in situ absorbance. *J. Chem. Phys.* 153(21):214902

Annual Review of
Physical Chemistry
Volume 74, 2023

Contents

Errata

An online log of corrections to *Annual Review of Physical Chemistry* articles may be found at http://www.annualreviews.org/errata/physchem